Vietnam Journal of Earth Sciences, 47(4), 589–606, https://doi.org/10.15625/2615-9783/23733

Vietnam Journal of Earth Sciences
https://vjs.ac.vn/index.php/jse

Horizontal crustal movements of the Red River Fault Zone in Vietnam from GPS Data (1994–2023)

Nguyen Viet Thuan[1,3], Ngo Van Liem[2*], Phan Trong Trinh[1], Nguyen Van Huong[2], Tran Van Phong[1,4], Nguyen Quang Xuyen[1]

[1]*Institute of Earth Sciences, VAST, Hanoi, Vietnam*
[2]*VNU University of Science, Vietnam National University, Hanoi, Vietnam*
[3]*School of Geodesy and Geomatics, Wuhan University, Wuhan 430079, China*
4 Graduate University of Science and Technology, VAST, Hanoi, Vietnam

Received 25 August 2025; Received in revised form 12 October 2025; Accepted 04 November 2025

ABSTRACT

This study analyzes horizontal crustal movements across the Red River Fault Zone (RRFZ), one of the major fault systems in northern Vietnam, using GNSS data collected over nearly 30 years (1994–2023). In the ITRF2008 reference frame, GNSS stations along the fault show an average East-Southeastward motion at a rate of approximately 32.65±0.4 mm/yr, consistent with the general movement of the South China (SC) block. A slight velocity difference of about 2.5 mm/yr between stations on the SC and Sundaland (SU) blocks indicates relatively stable regional tectonic conditions, although localized deformation persists. Relative velocity analysis between the two fault flanks reveals a right-lateral strike-slip rate of approximately 2±0.5 mm/yr, accompanied by a minor extensional component of about 1±0.3 mm/yr. These findings suggest a generally stable tectonic regime for the SC block, while also implying possible contributions from subsidiary fault structures or local deformation zones.

Keywords: Red River Fault Zone, GPS velocity, GNSS, Crustal deformation, Northern Vietnam.

1. Introduction

The Red River Fault Zone (RRFZ) is a primary active strike-slip fault system in Northern Vietnam, playing a crucial role in the region's tectonic evolution and geodynamic processes. It marks the boundary between the South China and Sundaland tectonic blocks. Numerous previous studies have demonstrated that this fault zone is directly associated with regional topographic development, seismicity, and crustal deformation (Tapponnier et al., 1986; Leloup et al., 1995; Trinh et al., 2012). As a result, the RRFZ has been the subject of extensive research, particularly in geology and tectonics, employing a variety of approaches and methodologies. These studies have shed light on multiple aspects of the geological, tectonic, and geomorphic evolution of the region during the Neogene-Quaternary period.

During the pre-Pliocene, the RRFZ was characterized by left-lateral strike-slip motion, as evidenced by numerous geological indicators along a discontinuous trace extending from southeastern Tibet to the Gulf of Tonkin (Tapponnier et al., 1990; Leloup et al., 1993, 1995, 2001). The total displacement along the fault has been estimated at

*Corresponding author, Email: liemnv@hus.edu.vn

700±200 km (Leloup et al., 1995), with tectonic activity dating back to at least ~34 Ma (Gilley et al., 2003). The transition from ductile to brittle deformation around 17 Ma marked a significant shift in the fault's evolution, after which the RRFZ remained largely quiescent until approximately 5.5 Ma (Trinh et al., 2012). Sinistral offset estimates along the fault range from 330±60 km (Lacassin et al., 1993) to 500–700 km (Leloup et al., 1995).

Since the Pliocene, the RRFZ has undergone a kinematic reversal, transitioning to a dextral strike-slip fault (Allen et al., 1984). This right-lateral movement is supported by diverse lines of evidence, including displaced streams, seismic and structural data, and repeated GNSS measurements. Estimates of total dextral offset vary considerably, ranging from 20–57 km (Allen et al., 1984), 40 km (Schoenbohm et al., 2005), to 200–250 km (Leloup et al., 1995). Quaternary offsets of individual valleys along the fault span from 6–9 km to more than 25 km (Allen et al., 1984; Replumaz et al., 2001; Schoenbohm et al., 2006), and reach up to 57 km in the Yunnan segment (Leloup et al., 1995; Wang et al., 1998). In the Vietnamese section, smaller-scale dextral displacements have been documented, ranging from 150–700 m (Trinh et al., 2012), 100–1300 m (Liem et al., 2011), and 0.3–2 km (Lacassin et al., 1994), to 400 m–5.3 km (Cuong and Zuchiewicz, 2001; Zuchiewicz et al., 2013). Corresponding Quaternary slip rates have been estimated at approximately 1–9 mm/yr (Allen et al., 1984) and 1–4 mm/yr (Weldon et al., 1994).

Regarding the study of modern tectonic displacement, several investigations and calculations have been conducted along the RRFZ and its adjacent regions. However, the results remain inconsistent, with noticeable discrepancies. Geodetic measurements suggest that current slip rates generally do not exceed 4 mm/yr (Cong and Feigl, 1999) or range from 0 to 3 mm/yr (To et al., 2001, 2013). Therefore, the extent and characteristics of the modern RRFZ movement require further investigation to better understand its kinematic mechanisms and geodynamic implications.

Nowadays, the Global Navigation Satellite System (GNSS) has become a vital tool in geodynamic research, enabling precise measurements of crustal displacement over time. This paper presents the results of GNSS data analysis collected along the RRFZ from 1994 to 2023, aiming to determine the fault's modern displacement. By processing and analyzing nearly three decades of GNSS data (1994–2023), this study seeks to elucidate the displacement characteristics, including slip rates and directions, thereby contributing to the assessment of tectonic movement trends and the kinematic behavior of this region. The results contribute to an improved understanding of the fault's current tectonic behavior and its implications for regional geodynamics.

2. Modern Tectonic Movement Setting

Research on modern crustal deformation and tectonic motion in Southeast Asia has attracted considerable scientific attention, particularly following the pioneering use of GPS initiated by Tregoning et al. (1994). Subsequent large-scale geodetic campaigns, such as the GEODYSSEA project, have significantly improved our understanding of regional geodynamics (Chamot-Rooke and Pichon, 1999; Michel et al., 2001). Notably, GPS analyses by Bock et al. (2003) confirmed that the Sundaland block is moving independently relative to the Eurasian plate. Similar GPS-based and seismic studies of crustal deformation have since been carried out in adjacent regions, including China (King et al., 1997; Wang et al., 2001; Shen et al.,

2005; Hu et al., 2007), Taiwan (Hsu et al., 2009), the Philippines (Galgana et al., 2007; Yu et al., 2013), and Thailand (Iwakuni et al., 2004).

Simons et al. (2007) synthesized a unified GPS velocity field covering Southeast Asia using ten years (1994–2004) of observations from over 100 stations across Indonesia, Malaysia, Thailand, Myanmar, the Philippines, and Vietnam. Their results indicate that the Sundaland block behaves as a rigid entity with a clockwise rotation pole located at 49.0°N, 94.2°E and a rotation rate of approximately 0.34°/Myr. Intra-block strain rates within Sundaland were generally estimated to be less than 7 nanostrain/year.

In Vietnam, GPS-based investigations of modern tectonic movements have also been undertaken. Based on GEODYSSEA data, To and Yem (2004) concluded that the Vietnamese territory is part of the Sundaland block, with a relative horizontal velocity of about 7 mm/yr, equivalent to a deformation rate of 15 nanostrain/year, representing an upper bound for horizontal crustal motion across Indochina. Cong et al. (2006) applied triangular strain analysis to assess horizontal displacement along the Red River and Lai Chau–Dien Bien fault zones. Trinh et al. (2011) utilized GPS data from four observation campaigns (2007–2010) from the East Vietnam Sea GPS network to characterize displacement trends and map deformation zones based on baseline length changes. These findings have been further refined by Trinh et al. (2015) and Huong et al. (2020), who assess crustal displacement and tectonic gradients in the Central Highlands and at the proposed site for the Ninh Thuan nuclear power plant. Minh et al. (2012, 2015) provided an integrated kinematic framework for the Indochina and Sundaland blocks. Stations across Southeast Asia were found to be moving generally southeastward, with northern Vietnamese stations (e.g., Hanoi, Hue) displaying faster velocities (32–35 mm/yr) compared to southern stations such as Ho Chi Minh City, NTUS (Singapore), and BAKO (Indonesia), which move at 22–26 mm/yr.

Lau et al. (2020) used GNSS data from 2016–2018 at seven CORS stations in Vietnam and three surrounding regional stations to determine tectonic velocities using the precise point positioning (PPP) technique with high reliability. The resulting velocities are consistent with existing plate-motion models and previous GPS observations, confirming the robustness of PPP for assessing contemporary tectonic deformation in Vietnam. Major stations such as Hanoi, Da Nang, and Ho Chi Minh City exhibit stable northeastward horizontal motions with magnitudes of approximately 27–33 mm/yr.

More recently, Trong et al. (2023) presented detailed results on crustal displacement using data from the continuously operating GNSS reference station network (CORS). By analyzing continuous GNSS time series from 55 CORS stations between 2018 and 2021 using Precise Point Positioning (PPP) and velocity modeling, they reported a coherent velocity field. All stations exhibited southeastward motion, with velocities ranging from 25.3 to 42.6 mm/yr and position accuracies between ±0.1 and ±1.0 mm/yr in the ITRF2014 frame.

Geodynamic analyses of the Red River Fault Zone from the Tibetan Plateau to the Vietnam border reveal spatial variations in tectonic activity. These differences allow the fault to be divided into three segments: the northern, middle, and southern segments.

The northern segment, located in the southern Tibetan Plateau and Yunnan region of China, is considered the most active. It exhibits a high degree of locking (Lu et al., 2021). GPS-based studies estimate a dextral strike-slip rate of approximately 4.7 mm/year,

significantly higher than in other parts of the fault. The combination of strong locking, elevated shear strain rates, and notable slip deficits suggests substantial stress accumulation, increasing the likelihood of moderate to strong earthquakes.

The southern segment may be experiencing slow aseismic creep, gradually releasing energy without generating large earthquakes. Nonetheless, the degree of locking here is reported to be lower than in the northern segment (Lu et al., 2021; Xuhua Shi et al., 2018).

In contrast, the middle segment is considered the least active, exhibiting low slip rates, minimal slip deficits, and weak indicators of strain accumulation. Accordingly, the probability of moderate-to-strong earthquakes in this region is considered low (Lu et al., 2021).

Turning to Northern Vietnam, To et al. (2013) analyzed GPS data from 27 stations collected between 1994 and 2007. Their results indicate that both the southwestern and northeastern sides of the Red River Fault Zone are moving eastward at a consistent rate of approximately 34.5±1 mm/yr, with slightly differing southward components of 12±1 mm/yr and 13±1 mm/yr, respectively, estimates of relative right-lateral slip velocity of the RRFZ from morphotectonic studies (along active fault zones in the Late Quaternary) (Trinh et al., 2012) show minor differences (about 0–3 mm/yr) between these two structures. Minh et al. (2020) quantified absolute crustal displacement at seven GPS sites, yielding southeast-to-east-southeast velocities ranging from 34.10±0.17 mm/yr to 35.05±0.18 mm/yr in the ITRF2014 reference frame. Relative motion analysis between MTEV and PHUT indicated a horizontal displacement rate of 3.78±0.19 mm/yr along a N45°W direction. Strain field analysis revealed extensional deformation ($\sim 10\times10^{-9}$/yr) west of the Song Ma Fault and compressional strain of similar magnitude west of the Da River Fault. Of particular note, the Son La Fault exhibited the highest left-lateral strike-slip strain ($\sim 30\times10^{-9}$/yr), consistent with a sinistral slip rate of 2.14±0.28 mm/yr. In contrast, the Da River and Song Ma Faults demonstrated dextral motion, with slip rates of 1.76±0.40 mm/yr and 2.44±0.47 mm/yr, respectively. Despite this coherent large-scale movement, differential motion across the Red River Fault Zone is relatively limited, often <4 mm/yr (To et al., 2001; Cong and Feigl, 1999), suggesting possible partial locking or slow creep.

These findings collectively highlight the RRFZ as a complex tectonic feature where long-term motion trends are consistent, but localized strain and slip rates vary. The discrepancies may reflect methodological differences, limited temporal coverage, or intrinsic fault behavior. This study, based on nearly three decades of continuous GPS data, aims to refine the understanding of crustal dynamics in Northern Vietnam and its tectonic context within Southeast Asia.

3. Materials and methods

3.1. GPS data

In this study, data were collected from ten GNSS stations (DOI1, HUN1, LAN0, LAP1, NAM0, NTH1, SOC1, SON1, XUY0, and VUA0), which were established in 1994 by the Institute of Geological Sciences now the Institute of Earth Sciences under the Vietnam Academy of Science and Technology (VAST), to study and evaluate active tectonic deformation along the RRFZ. The spatial distribution of these stations was determined based on tectonic and geological features as well as practical accessibility. Most stations are located along major geological structures associated with the RRFZ (Fig.1).

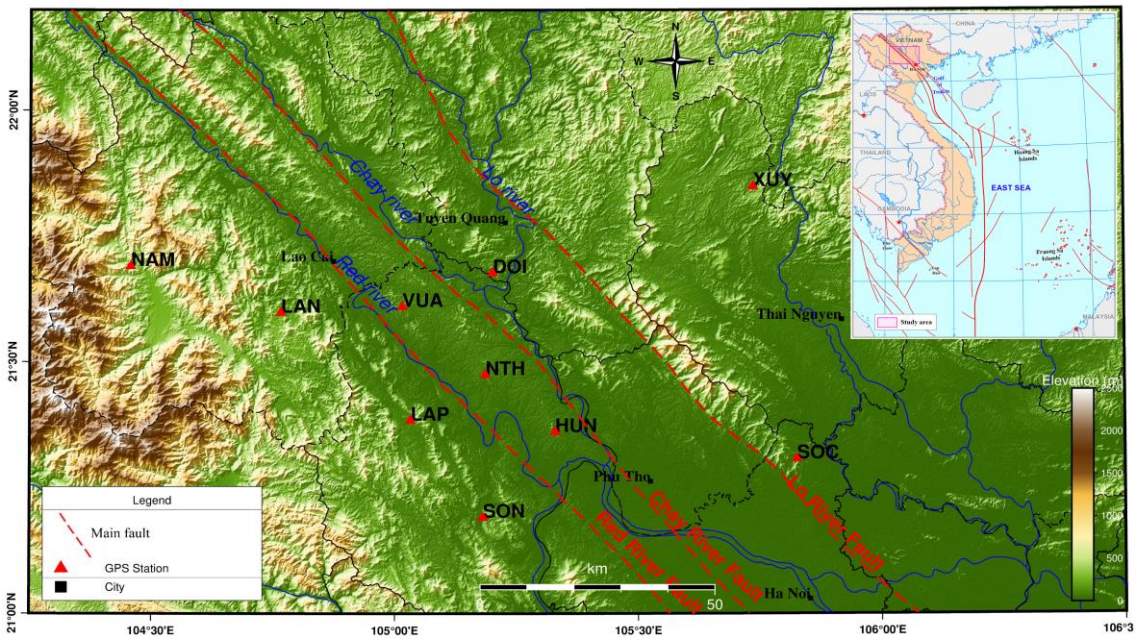

Figure 1. Map of GNSS stations in the study area

Data from these stations were obtained through eight repeated GNSS survey campaigns conducted between 1994 and 2023; an overview of these campaigns is presented in Table 1. Specifically, measurements from the 1994, 1996, 1998, 2000, 2006, and 2007 campaigns were sourced from previous studies (Cong and Feigl, 1999; Feigl et al., 2003; To and Cong, 2008; Hai et al., 2011). The 2010 survey was conducted under the national project "Neotectonics and Earthquake Hazards in Vietnam" (Project Code: 105.06.36.09), and the 2023 campaign was carried out within the framework of the national project Study on the Pliocene-recent tectonic geomorphology along the Red River-Chay River Fault Zones for the assessment of related geological hazards" (Project Code: ĐTĐL.CN-41/23).

Table 1. GNSS measurement data of the 1994–2023 cycles of the RRFZ network

Station name	Number of measurements / Measurement time/receiver type used							
	1994	1996	1998	2000	2006	2007	2010	2023
NAM	8/16/A			8/16/A			4/24/T	9/24/TR
LAN	4/16/A			4/16/A			4/24/T	4/24/L
NTH	4/16/A	2/8/A		4/16/A			4/24/T	4/24/TR
VUA	1/16/A			4/16/A	2/24/T		4/24/T	5/24/L
DOI	4/16/A			4/16/A			4/24/T	4/24/TR
XUY	8/16/A			8/16/A			12/24/T	9/24/TR
LAP	2/5/T	2/8/A	2/10/T	2/16/A	4/24/T			2/24/TR
SON	2/5/T	2/8/A	3/10/T	2/16/A	4/24/T	2/24/T		4/24/TR
HUN	4/5/T	6/8/A	9/10/T	2/16/A	10/24/T	2/24/T		4/24/TR
SOC	2/5/T	2/8/A	2/10/T	2/16/A	4/24/T			4/24/TR

A: Ashtech receiver; T: Trimble 400SSI/SSE receiver; TR: Trimble R9 receiver. L: Leica GR25

All campaigns followed a consistent, standardized data acquisition protocol: Dual-frequency receivers were used, with an elevation mask of 10° and a 30-second

sampling interval, and choke-ring antennas designed to minimize multipath interference. After each observation session, data were preliminarily reviewed in the field, edited and compiled, and then converted into RINEX format using the TeQC software (Estey and Meertens, 1999).

To estimate station velocities within the International Terrestrial Reference Frame 2008 (ITRF2008) (Altamimi et al., 2011), the RRF-GPS network was extended to include 15 global GNSS stations from the International GNSS Service (IGS), namely: ALIC, BAKO, BJFS, COCO, GUAM, IISC, KIT3, PERT, POL2, SHAO, SUWN, TIDB, TSKB, USUD, and WUHN. The availability of IGS data varied depending on the station's establishment dates and operational status. For example, in 1994, only a limited number of IGS stations in the Asia-Pacific region were available, including ALIC, TSKB, KIT3, PERT, IISC, and USUD.

3.2. GPS data processing

In this study, initial coordinates for each observation day were estimated using the Precise Point Positioning (PPP) method (Zumberge et al., 1997), as implemented in previous works (Nadia et al., 2021; Soycan, 2012). The average daily positions derived from the PPP solution were then used as a priori coordinates in the subsequent processing phase using the Bernese GNSS Software version 5.2. Providing accurate a priori coordinates accelerates the least-squares iterative solution by reducing the number of iterations when the initial approximation is close to the final solution.

Following the PPP step, data processing was performed using the standard procedure in Bernese GNSS Software 5.2 (Dach et al., 2017). Correction models and processing parameters applied at each stage are summarized in Table 2 (Danezis et al., 2020). The final station (ITRF2008) (Altamimi et al., 2011).

The ITRF2008 reference frame was adopted to ensure consistency and compatibility with global GNSS products and tectonic motion models, particularly those widely used in Southeast Asia (e.g., Simons et al., 2007; Kreemer et al., 2014). Although newer realizations of the ITRF (e.g., ITRF2014, ITRF2020) exist, ITRF2008 provides a stable and well-documented reference epoch that aligns with the temporal coverage of most RRF network campaigns (1994–2023). Moreover, many previous regional geodetic and tectonic studies in Indochina and southern China were also referenced to ITRF2008, facilitating direct comparisons and the integration of velocity results across datasets.

The Bernese software processes data under the assumption of a white noise model within a least-squares adjustment framework (Montillet et al., 2012). However, several studies have emphasized the impact of colored noise on velocity estimates, particularly for short or discontinuous time series (Soundy et al., 2020; He et al., 2021). Neglecting colored noise can lead to an underestimation of position and velocity uncertainties by up to a factor of 2 (Zhang et al., 1997; Klos et al., 2018; Williams, 2003). In the RRF network, identifying an appropriate stochastic noise model remains challenging due to limitations in the dataset. These include inconsistent temporal spacing between campaigns (ranging from 2 to 13 years), and variable observation durations and data continuity among stations. Consequently, it is difficult to distinguish between and apply a reliable colored-noise model, and the reported velocity uncertainties should be interpreted as lower-bound estimates. In future work, we intend to use more robust noise modeling and time series analysis techniques to improve the reliability of velocity estimates.

Table 2. Daily GNSS Data Processing Parameters and Settings in Bernese 5.2

Parameter	Setting	Input data
Observation type	GNSS carrier phase. Pseudo-range is used only for receiver clock synchronization and ambiguity resolution, and for linear combinations.	RINEX Observation files (.obs): GPS station of RRFZ network, IGS station.
Elevation cutoff angle	10°; observation weighting dependent on satellite elevation (cosz).	
Data sampling rate	30 seconds in the final solution.	
Observation modeling	Ionosphere-free linear combination to eliminate first-order ionospheric delay.	GNSS dual-frequency phase data
Antenna phase center corrections	Absolute Phase Center Correction (APC)	ANTEX files (igs20.atx)
Tidal corrections	- Solid Earth tides. - Ocean loading: FES2004 model.	IERS2010XY.SUB IAU2000R06.NUT http://ftp.aiub.unibe.ch/BSWUSER52/GEN/ FES2004 Model Data http://froste.oso.chalmers.se/loading/
Orbit and Earth Rotation Parameters (ERPs)	Final IGS precise orbits (GPS) and ERPs from CODE.	IGS Final Orbit (sp3) & ERP files. https://cddis.nasa.gov/archive/gnss/products http://ftp.aiub.unibe.ch/CODE
Ionospheric delay handling	First-order ionospheric delay is eliminated using the ionosphere-free L1/L2 linear combination. Regional ionospheric maps are used to enhance ambiguity resolution in the Quasi-Ionosphere-Free (QIF) method, as well as in L5/L3 and L1/L2 combinations.	COD***.ION http://ftp.aiub.unibe.ch/CODE
Ambiguity resolution	Ambiguities are resolved per baseline: -Quasi-Ionosphere-Free (QIF) method (2000 km). - Wide-lane phase-based method (< 200 km).	
Tropospheric delay modeling	- Dry GMF model (used as an a priori model). - Zenith total delay (ZTD) is estimated hourly for each station using wet GMF. - Horizontal tropospheric gradient estimated daily for each station following the Chen-Herring model.	VMF***.GRD https://vmf.geo.tuwien.ac.at/trop_products/GRID/2.5x2/VMF1/
Reference frame	ITRF2008	ITRF2008.CRD, ITRF2008.VEL, ITRF2008.FIX

To evaluate positional accuracy, we used the Weighted Root Mean Square (WRMS) of the coordinate components (Larson and Agnew, 1991; Fotiou et al., 2006), which reflects the repeatability of measurements at each station within each campaign. The WRMS is computed as follows (1):

$$Wrms_{N,E,H} = \sqrt{\frac{\frac{n}{n-1}\sum_{i=1}^{n}\frac{(y_i-\bar{y})^2}{\sigma_i^2}}{\sum_{i=1}^{n}\frac{1}{\sigma_i^2}}}, \quad (1)$$

where $\bar{y} = \frac{\sum_{i=1}^{n}\frac{1}{\sigma_i^2}y_i}{\sum_{i=1}^{n}\frac{1}{\sigma_i^2}}$ is the weighted mean of the observations y_i, y_i is the i-th observation, n is the number of independent values, and σ_i is the standard deviation of the i-th observation

We also assessed the accuracy of the baseline lengths using the model introduced by Savage et al. (1995) (2):

$$\sigma_{baseline} = \sqrt{(a^2 + bL^2)} \quad (2)$$

where a is the fixed error term (independent of baseline length), b is the scale-dependent error term, L is the baseline length, and $\sigma_{baseline}$ is the baseline uncertainty. The results are presented in Table 3.

Table 3. WRMS Repeatability and Baseline Length Precision in GPS Campaigns

Cycle	WRMS Repeatability (mm)			Precision of baseline length	
	N	E	H	a (mm)	b (ppb)
1994	0.98	1.03	1.98	2.20	0.55
1996	0.43	0.47	1.09	1.71	0.35
1998	0.52	0.48	1.23	2.18	0.44
2000	0.42	0.41	0.96	1.90	0.41
2006	0.25	0.24	0.60	1.66	0.25
2010	0.26	0.27	0.62	1.75	0.33
2023	1.01	1.05	1.75	2.11	0.47

Table 3 provides an overview of GPS data accuracy across all campaigns. Overall, the precision levels are within acceptable limits for geodetic applications. WRMS values remained stable from 1996 to 2010, whereas larger uncertainties were observed in the 1994 and 2023 campaigns, likely due to unmitigated noise. Several factors may have contributed to reduced accuracy in these specific years:

- Ionospheric model limitations: The use of a regional ionospheric correction model rather than a global one in 1994 (due to the absence of CODE global ionospheric products at that time) may have led to larger baseline errors, especially on long baselines.

- Changes in the observation environment: In 2023, decreased accuracy at the SON and HUN stations may be attributed to local environmental factors, such as nearby construction or radio interference, that affected signal quality.

A breakdown of baseline accuracy by length reveals that short baselines (<25 km) had uncertainties of approximately 2.2 mm (~0.098 mm/km), while the longest baseline (7455.7 km) exhibited an uncertainty of 5.32 mm (~0.00071 mm/km). These results suggest that for short baselines, the dominant error source is the fixed component aaa, typically associated with instrumentation or system noise. The scale-dependent component bL becomes more significant only for very long baselines (Cong et al., 2006).

According to International GNSS Service (IGS) standards (Dach et al., 2022), acceptable precision thresholds are: WRMS ≤ 1.5 mm for horizontal components (N, E), ≤ 2 mm for the vertical component (H), and baseline uncertainties of a ≤ 2.5 mm, b ≤ 0.5 ppb. Based on these criteria, the 2006 and 2010 campaigns yielded high-precision results, meeting the most stringent IGS standards. Campaigns in 1994, 1996, 1998, 2000, and 2023 also yielded usable data, though some error parameters slightly exceeded recommended values.

The study by Pham Le K. et al. (2024) used GNSS data to determine total precipitable water (TPW) in the Nghia Do area, showing only minor deviations from Aeronet and radiosonde measurements, thereby demonstrating the potential of GPS for atmospheric water vapor monitoring. Meanwhile, Nguyen Thanh D. et al. (2023) identified quasi-biennial oscillations (QBO) in the TEC amplitude of the two equatorial ionization anomaly crests over Southeast Asia, with periods of 18–30 months and a clear correlation with the tropospheric QBO. Most recently (Pham Thi Thu H. et al., 2024) investigated the occurrence rate of the Spread F phenomenon and the ROTI index at two GPS stations in Vietnam, revealing distinctive seasonal and nighttime variations characteristic of the equatorial ionization anomaly region. The results from these three studies help develop a spatiotemporal ionospheric correction model tailored for Vietnam, thereby reducing orbital and phase errors, improving the accuracy of GNSS positioning, and enhancing the reliability of derived products such as GPS velocity, TPW, and TEC.

4. Results

4.1. Absolute velocity results of the RRFZ GPS network

The results of absolute velocity estimations at the GPS stations along the RRFZ network are presented in Table 4. The data show a

general East-Southeastward motion across the study area, with an average velocity magnitude of 32.65±0.4 mm/year in the ITRF2008 reference frame. This trend is consistent with previous studies on tectonic movements in the region (Simons et al., 2007; Hai et al., 2016). The velocity uncertainty ellipses indicate relatively high and spatially uniform precision across the network. The horizontal velocity uncertainties in both the East and North components at most stations are 0.4–0.5 mm/year, suggesting reliable results. All velocity components VE and VN in the ITRF2008 frame have minimal uncertainties (±0.4–0.5 mm/yr), corresponding to a confidence level of about 95%. The VE component is slightly more reliable due to its larger magnitude, resulting in a smaller relative error. Therefore, the GPS velocities in ITRF2008 are highly reliable for analyzing block motion and comparing with Euler rotation models.

Table 4. Summary of Absolute Displacement Results of the RRFZ - GNSS Network Using Bernese 5.2 Software (ITRF2008)

TT	Station	Lon	Lat	VE ITRF 2008 (mm)	dVE Simons (mm)	dVE Satrio (mm)	dVE Ming (mm)	VN ITRF 2008 (mm)	dVN Simons (mm)	dVN Satrio (mm)	dVN Ming (mm)
1	**DOI**	105.201	21.677	32.22±0.4	-2.93	-2.06	-0.42	-10.09±0.4	-1.85	-3.79	-0.95
2	**HUN**	105.329	21.361	31.35±0.5	-3.74	-2.85	-1.24	-9.46±0.4	-1.16	-3.1	-0.28
3	**LAN**	104.766	21.598	30.73±0.4	-4.43	-3.55	-1.92	-8.23 ±0.4	-0.16	-2.12	0.77
4	**LAP**	105.032	21.383	30.89±04	-4.22	-3.33	-1.72	-8.28±0.4	-0.1	-2.05	0.8
5	**NAM**	104.457	21.690	30.83±0.4	-4.37	-3.48	-1.85	-6.15±0.4	1.79	-0.18	2.75
6	**NTH**	105.186	21.474	31.54±0.4	-3.58	-2.69	-1.07	-9.54±0.4	-1.3	-3.24	-0.41
7	**SOC**	105.826	21.307	31.16±0.4	-3.89	-3	-1.39	-8.25±0.4	0.25	-1.67	1.09
8	**SON**	105.181	21.191	30.43±0.5	-4.63	-3.73	-2.15	-10.23±0.4	-1.99	-3.93	-1.1
9	**VUA**	105.015	21.610	31.61±0.4	-3.54	-2.66	-1.03	-8.32±0.4	-0.15	-2.1	0.76
10	**XUY**	105.738	21.848	32.76±0.4	-2.4	-1.54	0.13	-12.55±0.4	-4.09	-6.01	-3.24

The azimuths of displacement vectors (ranging from N101° to N111°) show minor differences among stations. Still, the dominant movement direction remains East-Southeastward (Fig. 2). For tectonic analysis, the GPS stations are grouped into two clusters representing the South China Block (XUY, DOI, SOC) and the Sundaland Block (NAM, LAN, LAP, SON). This classification is based on the stations' geographic locations and regional geological structures: DOI, SOC, and XUY are located in the Northeastern part of the study area, belonging to the SC block, while NAM, LAN, LAP, and SON are situated in the Southwestern part, closer to the Sundaland margin. The analysis reveals that the average velocity magnitude of the SC group (~33.7 mm/year) is slightly higher than that of the SU group (~31.8 mm/year). The velocity difference of ~2 mm/year between the two blocks reflects a small but measurable divergence in absolute motion.

The values dVE Simons (mm), dVE Satrio (mm), and dVE Ming (mm) in Table 4 represent the deviations in the horizontal velocity component (in the East direction, VE) between the actual GPS observations in the ITRF2008 reference frame and the theoretical velocities predicted by the respective Euler pole models of Simons et al. (2007), Satrio et al. (2024), and Minghao et al. (2019).

In other words, these values indicate the discrepancy between model predictions and actual measurements of the East velocity component, thereby reflecting the degree of fit and each model's ability to describe tectonic motion in the study area.

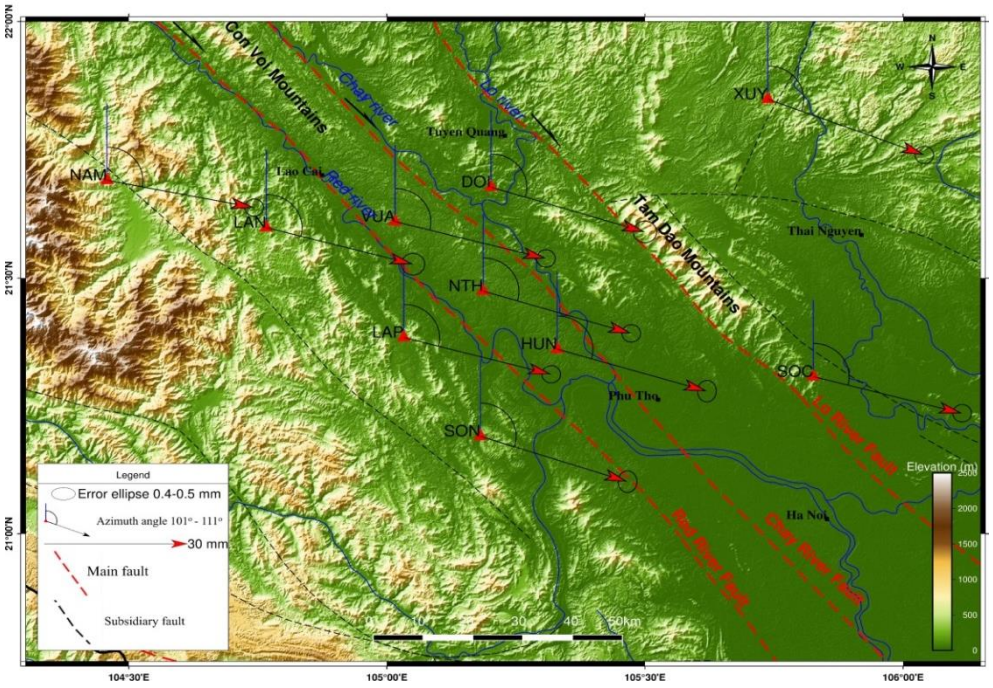

Figure 2. Absolute displacement velocity field

4.2. Relative velocity results across the RRFZ GPS network

To assess relative motion across the RRFZ, we fixed stations on either side of the fault and compared velocity vectors between the two groups. Two reference scenarios were considered: (a) fixing the South China (SC) group, and (b) fixing the Sundaland (SU) group.

As shown in Table 5 and illustrated in Fig. 3, clear relative displacements are observed between the two station groups:

In scenario (a), with the SC group fixed, stations NAM, LAN, LAP, SON, VUA, NTH, and HUN exhibit a dominant northwestward motion with an average velocity of approximately ~2 mm/year and an azimuth of ~N320°. Station SON shows a more westerly-oriented motion (~N272°).

Conversely, in scenario (b), with the SU group fixed, stations DOI, SOC, XUY, VUA, NTH, and HUN tend to move Southeastward, with an average relative velocity of ~1.8 mm/year and azimuth of ~N160°. Notably, VUA (~N96°) and SOC (~N93°) show significant deviation toward the East.

Table 5. Intergroup relative displacement

Station	Lon	Lat	(a)			(b)		
			VE	VN	Azimuth	VE	VN	Azimuth
DOI	105.20	21.67				1.5	-1.87	141.23°
HUN	105.32	21.36	-0.7	0.84	320.19°	0.63	-1.24	153.02°
LAN	104.76	21.59	-1.32	2.07	327.48°			
LAP	105.03	21.38	-1.16	2.02	330.13°			
NAM	104.45	21.69	-1.22	4.15	343.62°			
NTH	105.18	21.47	-0.5	0.76	326.14°	0.82	-1.32	148.10°
SOC	105.82	21.30				0.44	-0.03	93.58°
SON	105.18	21.19	-1.7	0.07	272.47°			
VUA	105.01	21.61	-0.44	1.98	347.47°	0.89	-0.01	96.25°
XUY	105.73	21.84				2.04	-4.4	154.76°

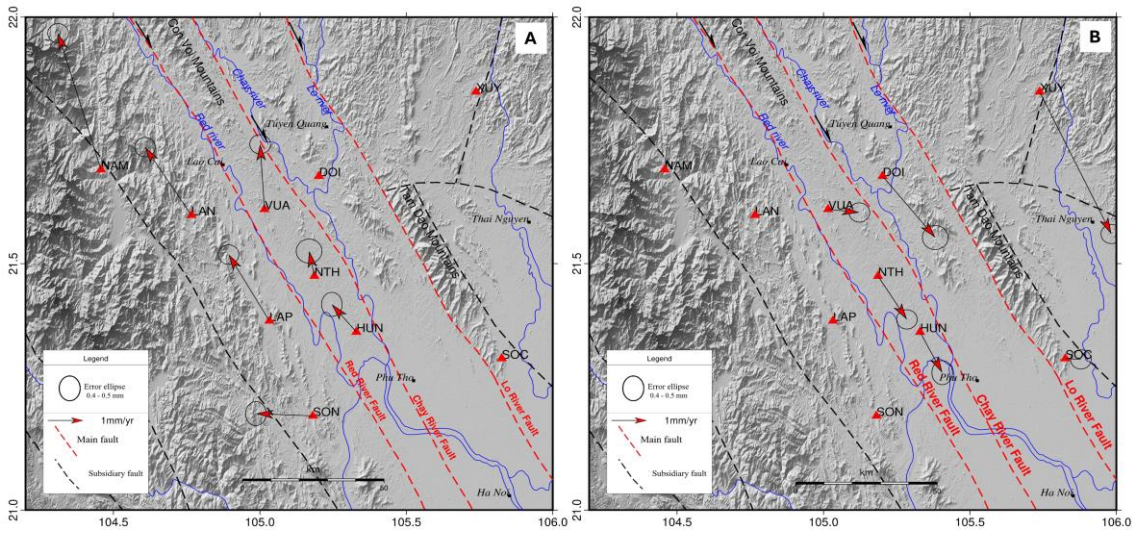

Figure 3. Relative displacements in two cases: (a) Fixing the points in group SC and (b) Fixing the points in group SU

Fault-block reference comparisons:

The relative symmetry of the motion vectors in the two scenarios suggests right-lateral strike-slip motion between the two tectonic blocks (Fig. 3). However, directional deviations at stations such as SON, SOC, and VUA may reflect internal deformation within the fault zone or the influence of secondary faults. Stations located within or near the RRFZ, such as VUA, HUN, and NTH, show apparent relative motion, though with lower velocity magnitudes. In contrast, stations farther from the fault zone, such as XUY and NAM, exhibit more pronounced velocity magnitudes, possibly indicating subtle extensional strain away from the core fault zone.

In both scenarios (a) and (b), stations VUA, NTH, and HUN are analyzed as dynamically responsive points, although they appear in both SC and SU groups. This is due to their location within or adjacent to the fault zone, where motions from both sides of the RRFZ influence them. Therefore, they are not rigidly classified into a single fault block, but instead function as sensitive markers of localized deformation and inter-block strain transfer.

The inclusion of these stations in both reference frames also allows cross-validation of the fault model by comparing variations in azimuth and velocity magnitude under different reference conditions. Specifically, these stations exhibit significant azimuthal differences between the two scenarios, underscoring their sensitivity to strike-slip dynamics and their importance for characterizing fault activity.

5. Discussions

Based on absolute and relative velocity estimates derived from GPS data analysis, we further examine and interpret the tectonic dynamics of the study area. Specifically, we perform quantitative comparisons of observed GPS velocities with previously published tectonic models and assess their consistency. In parallel, the relative velocities between GPS stations are utilized to characterize intra-block deformation trends and the kinematic behavior of the Red River Fault Zone (RRF) during the observation period.

5.1. Absolute Velocities

To clarify the regional kinematics and evaluate the compatibility of existing tectonic models with observational data, we compare the estimated GPS velocities with models proposed by Simons et al. (2007), Hao et al. (2019), and Satrio et al. (2024) (see Table 4).

Model-predicted velocities were computed using the respective Euler poles and transformed to a common reference frame (ITRF2000 or ITRF2014) using transformation parameters provided by the IERS (https://itrf.ign.fr/en/solutions/transformations). This ensures consistency in the coordinate framework used for comparison.

From the Euler poles defined in each model, we calculated predicted velocities at GPS stations and compared them with observed values. Discrepancies among models reflect not only methodological differences in data processing but also variations in tectonic deformation within the studied region.

To evaluate model performance, two statistical indices were used: mean absolute error (MAE) and root mean square error (RMSE) (Willmott & Kenji., 2005) (see Table 6). Results indicate that the Hao et al. (2019) model exhibits the best agreement with the observed GPS velocities, as evidenced by the lowest MAE and RMSE values among the three models.

Table 6. Evaluation criteria for model performance

Evaluation criteria (mm/yr)	**Simons (2007)**	**Minghao (2019)**	**Satrio (2024)**
MAE VN	1.28	1.21	2.81
MAE VE	3.77	1.29	2.88
RMSE VN	1.74	1.53	3.19
RMSE VE	3.83	1.43	2.96
Trend interpretation	Relatively stable	Well captures the trend	Shows signs of noise

Notably, the RMSE values are consistently higher than the MAE across all models, indicating larger individual errors that disproportionately influence overall accuracy. Among the evaluated approaches, the model of Satrio et al. (2024) exhibits the highest error metrics, which may reflect the impact of uneven spatial coverage of input data on the robustness of the Euler pole estimation.

Hao et al. (2019) established an independent reference frame for the SC block with Euler pole coordinates at 53.420°N, -101.102°W and a rotation rate of 0.311°/Myr in ITRF2008. The study concluded that the southern boundary of the SC block is relatively stable and exhibits limited deformation. The deviation of observed velocities from Hao's model indicates right-lateral strike-slip motion on both sides of the fault and minor deformation along the RRFZ, with a clockwise rotational trend.

When compared with previous velocity estimates in the region (e.g., Duong et al., 2013; To et al., 2013), our results show general agreement in both magnitude and azimuth (N101–N111°E). The slight velocity discrepancies (~1.5 mm/year) may result from differences in input data, processing techniques, and correction models used across studies. For instance, Duong et al. (2013) accounted for postseismic effects from major earthquakes such as the 2004 Sumatra and 2011 Tohoku events, which may influence velocity estimates. Overall, the absolute velocity results accurately reflect the general tectonic motion along the RRFZ, suggesting that the study area lies within the transitional zone between the SC and SU blocks but moves more coherently with the SC block.

Uncertainty considerations in velocity estimation:

Although the application of colored noise models (e.g., flicker noise or random walk noise) has been shown to significantly improve the reliability of velocity estimates in

continuous GNSS time series (Williams, 2003), such modeling remains challenging for campaign-mode GPS networks like the RRF. The temporal sampling of campaign data is typically too sparse to support stable estimation of stochastic noise parameters. In future work, we aim to improve the stochastic characterization of the RRF network by: (1) extending the observation period or increasing campaign frequency to build longer and more continuous time series; (2) applying advanced noise modeling approaches such as Allan variance analysis and maximum likelihood estimation (MLE), or utilizing specialized time series analysis tools (e.g., CATS, Hector, or the GAMIT/GLOBK time series module) to separate the white, flicker, and random-walk noise components; and (3) comparing results obtained under white and colored noise assumptions to assess the impact of noise models on velocity uncertainty. These improvements are expected to enhance the robustness of the velocity estimates and provide a more reliable basis for interpreting crustal deformation patterns in the study area.

5.2. Relative Velocities

Gan et al. (2021) estimated a total right-lateral slip rate along the RRFZ of 1.8–2.5 mm/year, with GPS-derived slip rates of 1–2 mm/year. Their results support a dominant right-lateral strike-slip mechanism, coupled with east-west extensional deformation and spatial heterogeneity along the fault trace. Lu et al. (2021), using CMONOC GPS station data spanning from Jianchuan to Hekou, found relative velocities indicating northwest-side motion of 4.7 mm/year, gradually decreasing southeastward, with minor extension (1–2 mm/year) perpendicular to the fault.

In line with our findings, the RRFZ exhibits both strike-slip and extensional components. To better quantify the deformation pattern, we applied a projection method that decomposed the relative velocities between GPS station pairs along the baseline connecting each pair. This approach isolates the velocity component parallel and perpendicular to the fault, enabling clearer identification of strike-slip and extensional behaviors.

We selected three station pairs NAM-XUY, LAN-DOI, and SON-SOC that represent different segments of the study area. These baselines were chosen to be approximately orthogonal to the main fault strike (N101E–N111°E) to optimize detection of extension components. The along-baseline component of relative velocity was computed as (3):

$$V|| = \overrightarrow{V_{rel}}.\hat{r}_{AB} \quad (3)$$

Where V_{rel} is the relative velocity vector from station A to B, and $\hat{r}_{AB}$ is the unit vector pointing from A to B. The quantity V|| is the scalar (dot) product of the relative velocity vector and the unit vector, yielding a scalar value.

This method allows for determining whether point B is moving toward or away from point A along a specific direction, parallel to the baseline. A positive value of V|| indicates an extensional trend, whereas a negative value suggests compression. It provides insights into whether two stations are converging or diverging along the spatial vector defined by the station pair.

Results show that all three baseline projections yield positive values: NAM-XUY: 1.05±0.3 mm/year, LAN-DOI: 1.1±0.3 mm/year, and SON-SOC: 1.1±0.3 mm/year. These consistently positive values indicate that the Eastern stations (XUY, DOI, SOC) are moving away from the Western stations (NAM, LAN, SON) in a direction roughly perpendicular to the fault. This consistent pattern reflects a mild extensional regime across the study area.

Combined with the relative velocity field, which confirms right-lateral strike-slip behavior along the RRFZ, our analysis reveals both lateral and extensional deformation components. The projected velocities

perpendicular to the fault underscore a secondary extensional motion, commonly observed in strike-slip fault zones subjected to an extensional stress field orthogonal to the primary slip direction. The estimated extension rate (~1.1 mm/year) and a dominant strike-slip motion (~2 mm/year) indicate a hybrid deformation regime. This behavior may be attributed to the interaction between right-lateral slip of the Southern RRFZ segment in China and localized extensional processes along its Eastern periphery. Furthermore, the spatial variability of slip rates along the fault, as reported by Gan et al. (2021), reflects the inherent complexity of tectonic activity in this region.

6. Conclusions

This study analyzed GNSS data collected between 1994 and 2023 to assess present-day crustal movements along the Vietnamese segment of the RRFZ, one of the most significant tectonic structures in northern Vietnam. The main findings are as follows:

- *Absolute motion*: GNSS stations along the RRF generally move toward the East-Southeast, with an average velocity of 32.65±0.4 mm/yr in the ITRF2008 reference frame. This motion is consistent with the movement of the South China block. A small velocity difference (~2 mm/yr) between stations situated on the South China and Sundaland blocks indicates relatively stable tectonics with minor localized deformation.

- *Relative motion*: Analysis of relative velocities between the two flanks of the fault reveals a predominant right-lateral strike-slip motion at a rate of approximately ~2±0.5 mm/yr, accompanied by a minor extensional component (~1±0.3 mm/yr) perpendicular to the fault. These results support a transtensional deformation regime, consistent with previous studies of the RRFZ.

- *Comparison with tectonic models*: The GPS results confirm that both the South China and Sundaland blocks exhibit relatively rigid motion with limited intraplate deformation. However, minor discrepancies between modeled and observed velocities may reflect the influence of subsidiary faults or local deformation zones.

- *Limitations and future directions*: Due to the discontinuous and spatially uneven nature of the campaign-mode GPS data, the results may be affected by uncorrected colored noise. Future work should incorporate continuous CORS data and employ more sophisticated noise models to improve velocity estimates and better constrain active deformation along the RRF.

Acknowledgments

The authors are grateful to T.D. To, V.Q. Hai, D.C. Cong, K.L. Feigl, B.V. Thom, H.Q. Vinh, and all other colleagues for their valuable discussions and dedicated contributions to the GPS survey campaigns conducted between 1994 and 2023. This research was carried out as part of the national project funded by the Ministry of Science and Technology of Vietnam (Project code: ĐTĐL.CN-41/23).

References

Allen C.R., Gillepie A.R., Han Y., Sieh K.E., Zhu C., 1984. Red River and associated faults, Yunnan province, China: Quaternary geology, slip rates, and seismic hazard. Geological Society of America Bulletin, 95(6), 686–700. https://doi.org/10.1130/0016-7606(1984)95%3C686:RRAAFY%3E2.0.CO;2.

Altamimi Z., Collilieux X., Metivier L., 2011. ITRF2008: an improved so-lution of the International Terrestrial Reference Frame. Journal of Geodesy, 85, 457–473. https://doi.org/10.1007/s00190-011-0444-4.

Bock Y., et al., 2003. Crustal motion in Indonesia from Global Positioning System measurements. J. Geophys. Res, 108(B8), 2367. https://doi.org/10.1029/2001JB000324.

Chamot-Rooke N., X. Le Pichon, 1999. GPS determined eastward Sundaland motion with respect to Eurasia confirmed by earthquakes slip vectors at Sunda and Philippine trenches. Earth. Planet. Sci. Lett., 173, 439–455. https://doi.org/10.1016/S0012-821X(99)00239-3.

Cong D.C., Yun H.-S., Cho J.-M., 2006. GPS measurements of horizontal deformation across the Lai Chau-Dien Bien (Dien Bien Phu) fault, in Northwest of Vietnam, 2002–2004. Earth, Planets and Space, 58, 523–528. https://doi.org/10.1186/BF03351949.

Cong D.C, Feigl K.L., 1999. Geodetic measurement of horizontal strain across the Red River Fault Zone near Thac Ba, Vietnam, 1963–1994. Journal of Geodesy, 73, 298–310. https://doi.org/10.1007/s001900050247.

Cuong N.Q., Zuchiewicz W.A., 2001. Morphotectonic properties of the Lo River Fault near Tam Dao in North Vietnam, Nat. Hazards Earth Syst. Sci., 1, 15–22, https://doi.org/10.5194/nhess-1-15-2001.

Dach R., Hugentobler U., Fridez P., Meindl M., 2017. Tutorial for Bernese GNSS Software Ver. 5.2. Astronomical Institute, University of Berne.

Dach Rolf, Brockmann, Elmar, et al., 2022. International GNSS Service: Technical Report 2022. https://doi.org/10.48350/179297.

Danezis C., Chatzinikos M., Kotsakis C.,2020. Linear and Nonlinear Deformation Effects in the Permanent GNSS Network of Cyprus. Sensors, 20(6), 1768. https://doi.org/10.3390/s20061768.

Duong N.A., Takeshi Sagiya., Fumiaki Kimata., Tran Dinh To., Vy Quoc Hai., Duong Chi Cong., Nguyen Xuan Binh., Nguyen Dinh Xuyen., 2013. Contemporary horizontal crustal movement estimation for northwestern Vietnam inferred from repeated GPS measurements. Earth Planets Space, 65, 1399–1410. https://doi.org/10.5047/eps.2013.09.01.

Estey L., Meertens C.C., 1999. TEQC: The Multi-Purpose Toolkit for GPS/GLONASS Data. GPS Solutions. GPS solution, 3, 42–49. https://doi.org/10.1007/PL00012778.

Feigl K.L., Duong Chi C., Becker M., Tran Dinh T., Neumann K., Nguyen Quang X., 2003. Insignificant horizontal strain across the Red River Fault Zone near Thac Ba, Vietnam from GPS measurements 1994–2000. Geophysical Research Abstracts 5. Paper Presented at the EGS-AGU-EUG Joint Assembly, Nice, France.

Fotiou A., Pikridas C., Chatzinikos M., 2006. Long distance GPS baseline solutions using various software and EPN data. GNSS Processing and Applications. Presented at the XXIII FIG Congress.

Galgana G., Hamburger M., McCaffrey R., Corpuz E., Chen Q., 2007. Analysis of crustal deformation in Luzon, Philippines using geodetic observations and earthquake focal mechanisms. Tectonophysics, 432(1–4), 63–87. https://doi.org/10.1016/j.tecto.2006.12.001.

Gan W., Molnar, P., Zhang, P., Xiao,G., Liang, S., Zhang, K., Li,Z., Xu, K., Zhang, L., 2021. Initiation of clockwise rotation and eastward transport of southeastern Tibet inferred from deflected fault traces and GPS observations. GSA Bull, 134, 1129–1142. https://doi.org/10.1130/B36069.1.

Gilley L.D., Harrison T.M., Leloup P.H., Ryerson F.J., Lovera O.M., Wang J.H., 2003. Direct dating of left-lateral deformation along the Red River shear zone, China and Vietnam. Journal of Geophysical Research, 103, B2. https://doi.org/10.1029/2001JB001726.

Hai V.Q., Cuong T.Q., Thuan N.V., 2016. Crustal movement along the Red River Fault Zone from GNSS data. Vietnam Journal of Earth Sciences, 38(1), 14–21. https://doi.org/10.15625/0866-7187/38/1/7846.

Hai V.Q., To T.D., Liem N.V., 2011. Determination of present crustal movements of Red River Fault Zone by the Tam Dao - Ba Vi GPS network (1994–2007). Vietnam Journal of Earth Sciences, 33(3), 474–479. https://doi.org/10.15625/0866-7187/33/3/438.

Hao M., Li Y., Zhuang W., 2019. Crustal movement and strain distribution in East Asia revealed by GPS observations. Sci Rep, 9, 16797. https://doi.org/10.1038/s41598-019-53306-y.

He Y., Nie G., Wu S., Li H., 2021. Analysis and Discussion on the Optimal Noise Model of Global GNSS Long-Term Coordinate Series Considering Hydrological Loading. Remote Sensing, 13(3), 431. https://doi.org/10.3390/rs13030431.

Hsu Y.J., Yu S.B., Simons M., Kuo L.C., Chen H.Y., 2009. Interseismic crustal deformation in the Taiwan plate boundary zone revealed by GPS observations, seismicity, and earthquake focal mechanisms. Tectonophysics, 479(1–2), 4–18. https://doi.org/10.1016/j.tecto.2008.11.016.

Hu X., Wang Q., Ma Q., Du X., 2007. Research and application of regional no-net-rotation reference frame. J. Geodesy & Geodynamics (in Chinese), 27, 52–60.

Huong N.V., Phong T.V., Trinh P.T., Liem N.V., Thanh B.N., Pham B.T., Bui D.T., Bieu N., Vinh H.Q., Xuyen N.Q., Tuc N.D., Thom B.V., Thuan N.V., Thao B.T., Phong L.H., Vinh V.D., Tan M.T., Hai V.Q., Lan N.M., Cuong T.Q., Son T.P.H., 2020.

Recent tectonics, geodynamics and seismotectonics in the Ninh Thuan Nuclear Power plants and surrounding regions, South Vietnam. Journal of Asian Earth Sciences, 187, 104080. https://doi.org/10.1016/j.jseaes.2019.104080.

Iwakuni M., Kato T., Takiguchi H., Nakaegawa T., Satomura M., 2004. Crustal deformation in Thailand and tectonics of Indochina peninsula as seen from GPS observations. Geophys. Res. Lett., 31. https://doi.org/10.1029/2004GL020347.

King R.W., Shen F., Burchfiel B.C., Royden L.H., Wang E., Chen Z., Liu Y., Zhang X.Y., Zhao J.X., Li Y., 1997. Geodetic measurement of crustal motion in southwest China. Geology, 25(2), 179–182. https://doi.org/10.1130/0091-7613(1997)025<0179:GMOCMI>2.3.CO;2.

Klos A., et al., 2018. On the combined effect of periodic signals and colored noise on velocity uncertainties. GPS Solut, 22, 1. https://doi.org/10.1007/s10291-017-0674-x.

Kreemer C., Blewitt G., Klein C.E., 2014. A geodetic plate motion and Global Strain Rate Model. Geochemistry, Geophysics, Geosystems, 15(10), 3849–3889. https://doi.org/10.1002/2014GC005407.

Lacassin R., Leloup P.H., Tapponnier P., 1993. Bounds on strain in large Tertiary shear zones of SE Asia from boudinage restoration. Journal of Structural Geology, 15, 677–692. https://doi.org/10.1016/0191-8141(93)90055-F.

Lacassin R., Tapponnier P., Leloup H.P., Trinh P.T., Yem N.T., 1994. Morphotectonic evidence for active movements along the Red River Fault Zone. In: Actes du Col- loque Internationale sur la sismotectonique et la risque sismique en Asie du Sud Est, Hanoi, 27, 66–71.

Larson K.M., Agnew D.C., 1991. Application of the Global Positioning System to crustal deformation measurement: 1. Precision and Accuracy. J. Geophys. Res., 96. https://doi.org/10.1029/91JB01275.

Lau N.N., Coleman R., Hoa H.M., 2020. Determination of tectonic velocities of some continuously operating reference stations (CORS) in Vietnam 2016-2018 by using precise point positioning. Vietnam Journal of Earth Sciences, 43(1), 1–12. https://doi.org/10.15625/0866-7187/15571 .

Leloup P.H, Lacasin, P. Tapponnier, U. Scharer, Zhong Dalai, Liu Xaohan, Zhangshan, Ji. Shaocheng, Phan Trong Trinh,1995. The Ailao Shan - Red Rive shear zone (Yunnan, China), Tertiary transform boundary of Indochina. Tectonophysics, 251, 3–84. https://doi.org/10.1016/0040-1951(95)00070-4.

Leloup P.H., Arnaud N., Lacassin R., Kienast J.R., Harrison T.M., Phan Trong T., Replumaz A., Tapponnier P., 2001. New constraints on the structure, thermochronology, and timing of the Ailao Shan-Red River shear zone, SE Asia. Journal of Geophysical Research, B, 106(B), 6683–6732. https://doi.org/10.1029/2000JB900322.

Leloup P.H., Harrison T.M., Ryerson F.J., Chen Wenji, Li Qi, Tapponnier P., Lacassin R., 1993. Structural, petrological and structural evolution of a Tertiary ductile strike-slip shear zone, Diancang Shan, Yunnan. Journal of Geophysical Research, 98, 6715–6743. https://doi.org/10.1029/92JB02791.

Liem N.V., Trinh P.T., Vinh H.Q., Huong N.V., 2011. Slip rates during the Middle-Late Pleistocene period along Red River Fault Zone in Lao Cai - Viet Tri section. Vietnam Journal of Earth Sciences, 33(3), 465–473 (in Vietnamese with English summary).

Lu X., Tan K., Li Q., Li C., Wang D., Zhang C., 2021. Analysis of the current activity of the Red River Fault Zone based on GPS data: new seismological inferences. Journal of Seismology, 25, 1525–1535. https://doi.org/10.1007/s10950-021-10033-0.

Metin Soycan, 2012. A Quality Evaluation of Precise Point Positioning within the Bernese GPS Software Version 5.0. Arabian Journal for Science and Engineering, 37, 147–162. https://doi.org/10.1007/s13369-011-0162-5.

Michel G.W., et al., 2001. Crustal motion and block behavior in SE-Asia from GPS measurements. Earth and Planetary Science Letters, 187(3–4), 239–244. https://doi.org/10.1016/S0012-821X(01)00298-9.

Minh L.H., Feigl K., Masson F., Cong D.C., Bourdillon A., Duchesne P.L., Thang N.C., Thanh N.H., Nam T.N., Lan H.T., 2010. Crustal motion from the continuous GPS data in Vietnam and in the Southeast Asian region. Vietnam J. Earth Sci., 32(3), 249–260. https://doi.org/10.15625/0866-7187/32/3/1026.

Minh L.H., Hung V.T., Hu J.-C., Minh N.L., Huang B.-S., Chen H.-Y., Thang N.C., Thanh N.H., Thanh L.T., Mai N.T., Hong P.T.T., 2020. Contemporary movement of the Earth's crust in the Northwestern Vietnam by continuous GPS data. Vietnam J. Earth Sci., 42(4), 334–350. https://doi.org/10.15625/0866-7187/42/4/15282.

Minh L.H., Masson R., Bourdillon A., Fleury R., Hu J.-C., Hung V.T., Thanh L.T., Thang N.C., Thanh

N.H., 2015. Recent crustal motion in Vietnam and in the Southeast Asia region by continuous GPS data. Vietnam J. Earth Sci., 36(1), 1–13. https://doi.org/10.15625/0866-7187/36/1/4132.

Montillet J-P., Tregoning P., McClusky S., Yu K., 2013. Extracting White Noise Statistics in GPS Coordinate Time Series, in IEEE Geoscience and Remote Sensing Letters, 10(3), 563–567. Doi: 10.1109/LGRS.2012.2213576.

Nadia A., Mahmoud Elhussien, Mostafa Rabah, Zaki Zidan, 2021. Assessment of NRCAN PPP online service in determination of crustal velocity: case study Northern Egypt GNSS Network. Arabian Journal of Geosciences, 14. https://doi.org/10.1007/s12517-021-06530-8.

Nguyen Thanh D., Le Huy M., Amory-Mazaudier C., Fleury R., Saito S., Nguyen Chien T., Le Truong T.. Hong Pham T.T., Thanh Nguyen H., Mai Nguyen T., Le Q., 2023. Ionospheric quasi-biennial oscillation of the TEC amplitude of the equatorial ionization anomaly crests from continuous GPS data in the Southeast Asian region. Vietnam Journal of Earth Sciences, 45(1), 1–18. https://doi.org/10.15625/2615-9783/17490.

Pham Le K., Nguyen Xuan A., Van Nguyen H., Hoang Hai S., Nguyen Nhu V., Bui Ngoc M., 2024. Precipitable water characterization using global navigation satellite system data: A case study in Nghia Do area, Vietnam. Vietnam Journal of Earth Sciences, 46(1), 82–99. https://doi.org/10.15625/2615-9783/19912.

Pham Thi Thu H., Christine Amory M., Le Huy M., Susumu S., Nguyen Thanh D., Luong Thi N., Luu V.H., Nguyen C.T., Nguyen T.H., Michi N., Septi P., 2024. Occurrence rate of equatorial Spread F and GPS ROTI in the ionospheric anomaly region over Vietnam. Vietnam J. of Earth Sciences, 46(4), 553–569. https://doi.org/10.15625/2615-9783/21368.

Replumaz A., Lacassin R., Tapponnier P., Leloup P.H., 2001. Large river offsets and Plio-Quaternary dextralstrike-slip rate on the Red River Fault Zone (Yunnan, China). Journal of Geophysical Research, 106, 819–836. https://doi.org/10.1029/2000JB900135.

Satrio M.A., Ching K., Sagiya T., Wahyuni W.N. 2024. Determination of Euler pole parameters for Sundaland plate based on updated GNSS observations in Sumatra, Indonesia. Geoscience Letters, 11. https://doi.org/10.1186/s40562-024-00330-0.

Savage J.C., et al., 1995. Strain accumulation in Owens Valley, California, from 1974 to 1988. Bulletin of the Seismological Society of American, 85, 151–158. https://doi.org/10.1785/BSSA0850010151.

Schoenbohm L.M., Burchfiel B.C., Liangzhong C., Jiyun Y., 2005. Exhumation of the Ailao Shan shear zone recorded by Cenozoic sedimentary rocks, Yunnan Province, China, Tectonics, 24, TC6015. Doi: 10.1029/2005TC001803.

Schoenbohm L.M., Brchfiel B.C., Liangzhong C, Jiyun Y., 2006. Miocene to present activity along the Red River Fault Zone, China, in the context of continental extrusion, upper-crustal rotation, and lower-crustal flow. GSA Bullentin, 118, 672–688. https://doi.org/10.1130/B25816.1.

Shen Z.K, Lu J., Wang M., Burgmann R., 2005. Contemporary crustal deformation around the southeast borderland of the Tibetan Plateau. J. Geophys. Res., 110. https://doi.org/10.1029/2004JB003421.

Simons W.J.F., Socquet A., Vigny C., Ambrosius B.A.C., Haji Abu S., Chaiwat Promthong, Subarya C., Sarsito D.A., Matheussen S., Morgan P., Spakman W., 2007. A decade of GPS in Southeast Asia: Resolving Sundaland motion and boundaries. Journal of Geophysical Research, 112. https://doi.org/10.1029/2005JB003868.

Soundy A.W.R., Panckhurst B.J., Brown P., Martin A., Molteno T.C.A., Schumayer D., 2020. Comparison of Enhanced Noise Model Performance Based on Analysis of Civilian GPS Data. Sensors, 20(21), 6050. https://doi.org/10.3390/s20216050.

Tapponnier P., Peltzer G., Armijo R., 1986. On the mechanics of the collision between India and Asia. in Coward, M.P, and Ries, A.C., eds., Collision Tectonics, Geological Society Special Publication, 19, 115–157.

Tapponnier P., Lacassin R., Leloup P.H., Schirer U., Zhong D., Liu X., Ji S., Zhang L., Zhong J., 1990. The Ailao Shan/Red River metamorphic belt: Tertiary left-lateral shear between Indochina and south China. Nature, 343, 431–437.

To T.D, Yem N.T., 2004. Modern movements of the earth's crust of Vietnam territory according to GPS measurements. Vietnam Journal of Earth Sciences, 26(4), 579–586.

To T.D, Cong D.C., 2008. Absolute motion of the Red River Fault Zone system area (from Yen Bai to Thai Nguyen) deducted from GPS data.

Vietnam Journal of Earth Sciences, 30(4), 374–379. https://doi.org/10.15625/0866-7187/30/4/11771.

To T.D., Yem N.T., Cong D.C., Hai V.Q., Zuchiewicz W., Cuong N.Q., Nghia N.V., 2013. Recent Crustal movements of northern Vietnam from GPS data. Journal of Geodynamics, 69, 5–10. https://doi.org/10.1016/j.jog.2012.02.009.

To T.D., Yem N.T., Feigl K., Cong D.C., Hai V.Q., 2001. The activity of Red River Fault Zone derived from GPS data. Journal of Earth Sciences, 23(4), 436–441.

Tregoning P., Brunner F.K., Bock Y., Puntodewo S.S.O., McCaffrey R., Genrich J.F., Calais E., Rais J., Subarya C., 1994. First geodetic measurement of convergence across the Java trench. Geophys. Res. Lett., 21, 2135–2138.

Trinh P.T., Liem N.V., Hai V.Q., Phong T.V., Huong N.V., Thuan N.V., Xuyen N.Q., Thom B.V., Tuc N.D., Vinh H.Q., Thinh N.H., Thao B.T., Hung T.Q., 2015. Present day tectonic gradient in Ninh Thuan and surrounding region. Vietnam Journal of Marine Science and Technology, 15(3), 209–224. https://doi.org/10.15625/1859-3097/15/3/7216.

Trinh P.T., Liem N.V., Huong N.V., Vinh H.Q., 2011. Velocity of actual tectonic movement in east Vietnam sea and surrounding from GPS measurement 2007-2009. Journal of Marine Science and Technology, 11, 15–30. https://doi.org/10.15625/1859-3097/15/2/6499.

Trinh P.T., Liem N.V., Huong N.V., Vinh H.Q., Thom B.V., Thao B.T., Tan M.T., Hoang N., 2012. Late Quaternary tectonics and seismotectonics along the Red River Fault Zone, North Vietnam. Earth-Science Reviews, 114, 224–235. https://doi.org/10.1016/j.earscirev.2012.06.008.

Trong T.D., Nguyen D.H., Vu N.Q., Nguyen Q.L., 2023. Crustal displacement in Vietnam using CORS data during 2018-2021. Earth Sciences Research Journal, 27(1), 27–36. https://doi.org/10.15446/esrj.v27n1.102630.

Wang E., Burchfiel B.C., Royden L.H., Liangzhong Ch., Jishen Ch., Wenxin L., Zhi-Liang Ch., 1998. Late Cenozoic Xianshuihe-Xiaojiang, Red River, and Dali Fault systems of Southwestern Sichuan and Central Yunnan. Geological Society of America, China, 327p.

Wang Q., Zhang P.Z., Freymueller J.T., Bilham R., Larson K.M., Lai X., You X., Niu Z., Wu J., Li Y., Liu J., Yang Z., Chen Q., 2001. Present-day crustal deformation in China constrained by Global Positioning System measurements. Science, 294. https://doi.org/10.1126/science.1063647.

Weldon R., Sieh K., Zhu C., Han Y., Yang J., Robinson S., 1994. Slip rate and recurrence interval of earthquake on the Hong He (Red River) Fault, Yunnan. International Workshop on Seismotectonics and Seismic hazard in SE Asia, P.R.C, 244–248.

Williams S., 2003. The effect of coloured noise on the uncertainties of rates estimated from geodetic time series. Journal of Geodesy, 76, 483–494. https://doi.org/10.1007/s00190-002-0283-4.

Willmott, Matsuura, 2005. Advantages of the mean absolute error (MAE) over the root mean square error (RMSE) in assessing average model performance. Climate Research, 30, 79–82. https://doi.org/10.3354/cr030079.

Xuhua Shi, Kerry Sieh, Ray Weldon, Chengnan Zhu, Yuan Han, Jiwu Yang, Stephen W. Robinson, 2018. Slip Rate and Rare Large Prehistoric Earthquakes of the Red River Fault, Southwestern China. Geochemistry, Geophysics, Geosystems, 19(7), 2014–2031. https://doi.org/10.1029/2017GC007420.

Yu S.B., Hsu Y.J., Bacolcol T., Yang C.C., Tsai Y.C., Solidum R., 2013. Present-day crustal deformation along the Philippine Fault in Luzon, Philippines. Journal of Asian Earth Sciences, 65, 64–74. https://doi.org/10.1016/j.jseaes.2010.12.007.

Zhang J., Yehuda Bock, Hadley Johnson, Peng Fang, Simon Williams, Joachim Genrich, Shimon Wdowinski, Jeff Behr, 1997. Southern California permanent GPS geodetic array: Error analysis of daily position estimates and site velocities. Journal of Geophysical Research, 102, 035–18,055. https://doi.org/doi:10.1029/97JB01380.

Zuchiewicz W., Cuong N.Q., Zasadni J., Yem N.T., 2013. Late Cenozoic tectonics of the Red River Fault Zone, Vietnam, in the light of geomorphic studies. Journal of Geodynamics, 69, 11–30. https://doi.org/10.1016/j.jog.2011.10.008.

Zumberge M.B., Heflin D.C., Jefferson M.M., Watkins F.H. Webb, 1997. Precise point positioning for the efficient and robust analysis of GPS data from large networks. Journal of Geophysical Research, 102, 5005–5017. https://doi.org/doi:10.1029/96JB03860.